

# Automatic Pupil Detection in Ophthalmology Diagnosis

Wei-Jun Chen  
 Carl Zeiss Meditec AG  
 Göschwitzer Straße 51-52,  
 Jena, Germany  
 wei-jun.chen@zeiss.com

## Abstract

*Automatic pupil detection is often required as a necessary function in modern Ophthalmology diagnosis. After analyzing the major challenges existing in various diagnosis environments, this paper suggests a stepwise work-flow combining machine vision algorithms including spatial convolution, circular Hough transform and region growing, to provide robust and precision alignment between diagnostic system and patient's pupil. Experiments on a large scale image data-set as well as on live devices show that critical requirements in clinic diagnosis have been satisfied.*

## 1 Introduction

Ophthalmology diagnosis often needs to closely observe a patient's eye and pupil. As clinic key data, biometric measurements, for instance, the axial length, the corneal curvature, the corneal thickness, etc., must be accurately measured. Because these measurements conceptually depend on the alignment between two optical axes (one for the human eye and another one for the measuring system), it is vital to obtain and keep such an alignment during a measuring period. For higher level of robustness, accuracy, and efficiency in clinic diagnosis, automatic pupil detection/alignment is frequently required.

The problem of object detection has been exhaustively investigated for decades in the field of machine vision [1]. Particularly for automatic human pupil detection, plenty of methods together with their hardware design have been suggested in at least three different areas. Required by intelligent human-machine interface, eye/pupil tracking techniques based on dark/bright pupil caused by off-axis or on-axis infrared (IR) illumination have been addressed for a long time [5] [6], where image difference method is often adopted for stronger pupil signal. Extending these concepts with multiple light sources, multiple pupil detection/tracking is also possible [7]. Other than eye tracking techniques estimate pupil center in a coarse scale, iris recognition based personal identification requires more accurate pupil localization and pupil/iris segmentation [8], where algorithms including Graph cuts [9], circle/ellipse fitting [10], Circular Hough transform [11], and so on, are widely employed for precise pupil boundary description. Many pupil detection methods have also been suggested for clinic applications. Examples include pupil parameter estimation for eye fixation/micro-movement analysis [12], active contour based pupil descriptor for diagnosing bipolar disorder [13], pupil segmentation and contour extraction for Ophthalmology applications [14], so on and so forth.

Although many methods have been already suggested for pupil detection, all of them are either strongly hardware dependent, or imaging condition limited. By the way, all the above methods work on focused images, where system focusing is assumed to be fulfilled before pupil detection.

The environment for Ophthalmology diagnosis is often unpredictable. It might be under the sun shine, or might be in a dark room, with or without a desk lamp. Also, the short observing distance makes it easy to lose the optical focus. Moreover, an existing diagnostic device normally has already its success market, its medical certifications, and its mature system design. It is natural to be asked that hardware modifications should be minimized when adding a new software module such as pupil alignment.

As a medical application in Ophthalmology, this paper suggests a stepwise work-flow combining algorithms of spatial convolution [2], circular Hough transform [3], and region growing [1] together, for automatic pupil detection and pupil/system alignment. The spatial convolution decomposes a source image into scale dependent components; the circular Hough transform picks out characteristic object from a parameter space; the region growing algorithm figures out a pupil region from the image; based on these stepwise results, system focusing level and the pupil/system alignment level are further evaluated.

The rest of this paper will be organized as following: In next section, the problem faced in this paper will be clarified together with a short system description; In Section 3 the work-flow as well as stepwise measurements will be introduced in details; Experiments will be described in Section 4; Two points will be discussed in Section 5; Finally Section 6 concludes this paper.

## 2 System description

A diagnostic device in Ophthalmology normally includes a pupil/eye imaging module using a video camera. An active illumination by infrared LEDs (Light Emitting Diodes) is often adopted for better and consistency clinic observation under various environments. LEDs are often peripherally placed surrounding the system lens for illumination uniformity. Fixation point or object is designed for patients to fix their eyes by gazing on it. The diagnostic device could be adjusted in  $(x, y, z)$  space (Fig.1) for axis alignment between the imaging module and a measured eye. A measuring action is triggered when a satisfied alignment is achieved, which is evaluated based on individual video frames (Fig.2), where distinct three parts: the dark pupil, the gray iris, and the relatively bright (white) sclera, are included together with the cornea reflection of the IR

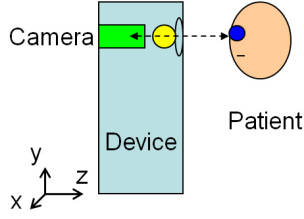


Figure 1. An Ophthalmology diagnosis.

LEDs<sup>1</sup>. If the two optical axes are aligned, the dark pupil region should be covered by LED spots. Otherwise, LED spots and the pupil region are deviated from each other, as shown in Fig.2(a) and Fig.2(b).

### 3 Pupil detection/alignment

Aligning a diagnostic device with an eye is equivalent to answer questions: 1), Where are the LED spots? 2), How good those spots are? 3), Is there a pupil nearby those spots? 4), Is the pupil sharp enough? 5), Is the pupil properly covered by LED spots?

A four-step work-flow is suggested to answer these questions: content decomposition, infrared spot detection, pupil detection and alignment evaluation.

**Content decomposition:** It is widely accepted that a shading pattern caused by imperfect optics mainly occupies low frequencies in the frequency domain. On another hand, infrared spots are designed to be small, but always bright spots in an observed image.

Given an observed image,  $\mathcal{I}$ , its low frequency component,  $\mathcal{I}_s$ , could be generated by a spatial convolution

$$\mathcal{I}_s(x, y) = \mathcal{I}(x, y) \otimes w(x, y|l_s), \quad (1)$$

where  $w(x, y|l_s)$  is a two dimensional window function given its window size  $l_s$ . The shading free content  $\mathcal{I}_f$  could be estimated by

$$\mathcal{I}_f(x, y) = \mathcal{I}(x, y) / \mathcal{I}_s(x, y), \quad (2)$$

where a multiplicative shading is assumed(Fig.3(b)).

Given a smaller window size,  $l_m$ , we may get

$$\mathcal{I}_f^m(x, y) = \mathcal{I}_f(x, y) \otimes w(x, y|l_m). \quad (3)$$

The bright spots are then characterized as  $\mathcal{I}_t$ :

$$\mathcal{I}_t(x, y) = \begin{cases} \frac{\mathcal{I}_f(x, y) - \mathcal{I}_f^m(x, y)}{\mathcal{I}_f^m(x, y)}, & \text{if } \mathcal{I}_f(x, y) > \mathcal{I}_f^m(x, y) > \delta_t \\ 0, & \text{otherwise} \end{cases}, \quad (4)$$

where factor  $\delta_t > 0$ , for avoiding extreme values.

**Infrared spots:** Six infrared spots are designed peripherally placed on a virtual circle, specified by its center  $\vec{x}_c \equiv (x_c, y_c)$ , and its radius  $r_c$ . The circular Hough transform is chosen as a spot detector:

$$(\vec{x}_c, r_c) \equiv (x_c, y_c, r_c) = \arg \max_{x, y, r} h(x, y, r), \quad (5)$$

<sup>1</sup>The situation that an eye is totally outside the imaging scope will not be addressed in this paper.

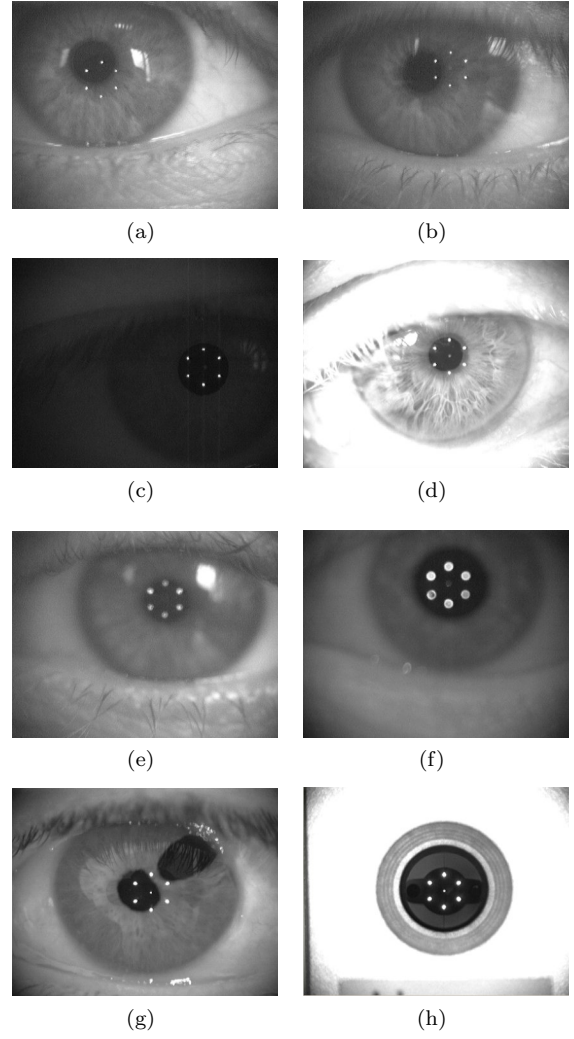


Figure 2. Typical images in clinic diagnosis: (a)–(g) observed images with various environmental illuminations; (h) model-eye for system calibration.

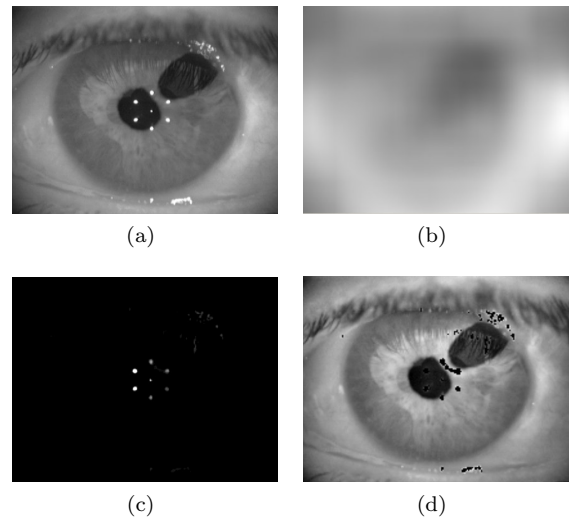


Figure 3. Scale dependent components in an observed image: (a), the source image; (b), the global shading; (c), the spot map; (d), the eye content without shading and spots.

where

$$h(x, y, r) = \sum_{|(x', y') - (x, y)| = r} \mathcal{I}_t(x', y') \quad (6)$$

maps  $\mathcal{I}_t$  onto a parameter space  $h$ .

The quality of infrared spots is measured based on an one-dimensional curve,  $\mathcal{C}_s(\theta)$ , as

$$\mathcal{C}_s(\theta) = \sum_{r' \leq r \leq r''} \mathcal{I}_t(r, \theta | \vec{x}_c), \quad (7)$$

where  $r' < r_c$  and  $r'' > r_c$ , denote the radius range of pixels contributing to the arc-length projection in Eq.7.  $(r, \theta)$  denote polar coordinates, where we have  $r = |\vec{x} - \vec{x}_c|$ ,  $x = r \cos \theta$ , and  $y = r \sin \theta$ .

The curve  $\mathcal{C}_s(\theta)$  for Fig.3(c) and its normalized version are shown in Fig.4(a) and Fig.4(b). Based on the normalized curve, the spot quality is evaluated as the average width of 6 peaks.

**Pupil:** A pupil is normally observed as a dark region nearby the infrared spots. Initially a dark seed  $\vec{x}_d \equiv (x_d, y_d)$  as the pixel with minimum value nearby the detected spots should be found on the shading free image  $\mathcal{I}_f$  (Fig.3(d)), a region with one pixel,

$$\Delta \equiv \Delta_0 = (x_d, y_d), \quad (8)$$

and its boundary  $\Omega \equiv \Omega_0$  could be identified. A region growing algorithm

$$\Delta_{i+1} = \Delta_i \cup \{b_i\}, \quad (9)$$

$$\Omega_{i+1} = (\mathcal{I}_f - \Delta_{i+1}) \cap (\Delta_{i+1} \oplus 1) \quad (10)$$

is suggested as a two-step procedure (where  $\oplus$  denotes a dilation operation). The candidate pixel to be added into a pupil is picked out by

$$b_i = \begin{cases} \arg \max_{b \in \Omega_i} p(b | \Delta_i), & \text{if } i < N_r \text{ or } p > \delta_r \\ \text{null}, & \text{otherwise} \end{cases} \quad (11)$$

where  $p(b | \Delta_i)$  denotes the probability of a boundary point  $b$  being added into the  $i$ th pupil region.  $N_r$  gives out a minimum number of pixels for estimating the value distribution of  $\Delta_i$ , and  $\delta_r$  is a threshold used as stop condition.

The sharpness of a detected pupil (e.g. Fig.5) is estimated as the average gradient of its boundary points.

**Alignment:** The alignment between two axes is determined based on a basic assumption, that a pupil has a simply round shape thus that could be roughly covered by an ellipse. The alignment measure is defined as

$$\mathcal{A} = \begin{cases} |(x_p, y_p) - (x_c, y_c)|, & \text{if } \mathcal{Q} > \delta_a^c \text{ and } |\Delta| > \delta_a^p \\ \infty, & \text{otherwise} \end{cases}, \quad (12)$$

where  $(x_p, y_p)$  denotes the center of an ellipse covering the detected pupil,  $\mathcal{Q}$  and  $|\Delta|$  denote the spot quality and the pupil size respectively (which should be larger than two thresholds  $\delta_a^c$  and  $\delta_a^p$ ). If two optical axes are aligned to each other, the distance between two centers, say, the center of a pupil and the center of infrared spots, should be small.

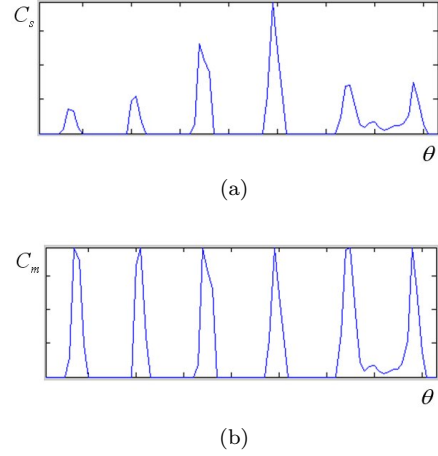


Figure 4. LED spot quality: (a), the curve from an arc-length projection based on the detected circle; (b), its normalized curve for spot quality evaluation.

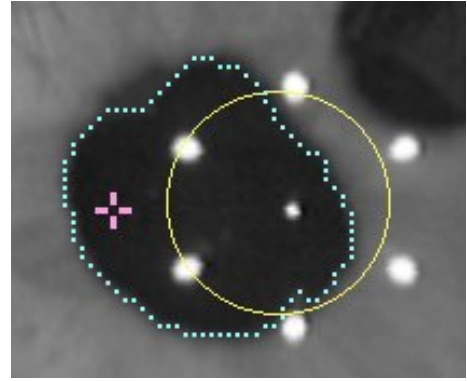


Figure 5. Pupil detection: the virtual LED circle, the dark seed and the estimated pupil boundary.

## 4 Experiments

**Experiments on still images:** The data-set of 1260 still images includes 255 images for system-test-eyes (Fig.2(h)), 217 images for very bright environment, 421 for very dark environment, and 546 images for variously out-focused pupils. About 300 human eye images were taken from 23 named persons by one prototype device, and other images were taken from anonymous patients by other 8 pre-production devices. Being tested on the targeting system (Intel(R) Core(TM)2 Dual CPU (2.40GHz), 2GB RAM, Windows XP Professional OS), the suggested work-flow averagely spent 0.0645 second per image, where 0.235 second was the maximum.

The robustness and accuracy of the workflow were evaluated by stepwise FALSE ratios (Table 1), where a FALSE signal inside the workflow means its results give out wrong suggestion to clinic doctors.

**Experiments on live videos:** Live video tests were performed on 9 production devices, where pupil detection work-flow was integrated into an automatic measuring procedure. Experiments on live devices have shown a great success both for system test eyes

Situations	SC(%)	SQ(%)	PF(%)	AD(%)
test eyes	5.1	3.1	11.4	3.1
human eyes	0.9	0.8	4.3	0.8
bright illum.	1.4	0.5	0.8	0.5
dark illum.	1.2	1.0	10.7	1.0
normal illum.	1.3	1.8	1.4	1.8
prototype	0.6	0.4	0.8	0.6
other devices	2.7	2.0	0.8	1.9
focused	1.0	1.1	0.9	0.9
out-focused	2.7	1.5	6.5	1.8
total	1.8	1.3	8.5	1.4

Table 1. Algorithm false ratio on individual steps: SC(spot center), SQ(spot quality), PF(pupil focus) and AD (Alignment decision).

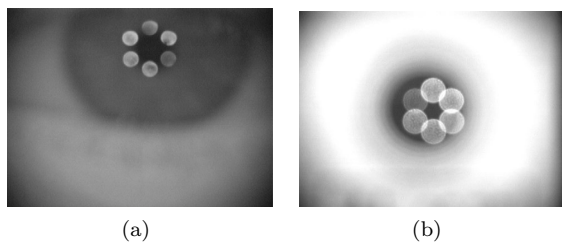


Figure 6. Mis-leading sharp edges for automatic pupil focusing.

and for more than 50 human patients, with various environmental illuminations.

## 5 Discussions

Other than usually working on binary edge points, in this paper the Hough transform works on gray level data together with additional considerations [4]: a), the signal of a targeting object should be strong enough to result in a dominate peak in the object parameter space; b), the object detection is biased (Fig.5) because of the various gray values; c), for efficiency, mapping large amount of pixels should be avoided.

Unlike popular auto-focusing methods based on analyzing the image frequency, this paper evaluates the focusing level by infrared spot quality and the pupil boundary sharpness. The motivation of this is to avoid mis-leading sharp edges, as shown in Fig.6(a) and 6(b), where specular (corneal) reflection always generates sharp edges which are irrelevant to optical focus.

## 6 Conclusions

Aiming at automatic alignment between a measuring device and its measured eye, pupil detection problem in Ophthalmology diagnosis has been clarified in this paper. A four-step work-flow combining popular machine vision algorithms has been suggested. Working with such a work-flow, an observed image is decomposed into global shading, bright spots, and a human eye image. Characterizing features including infrared

spots and dark pupil could be detected and evaluated. Experiments on both still images and live diagnostic devices show that the suggested work-flow successfully satisfies major requirements in clinic applications, thus that be greatly helpful for flexible, precision and robust Ophthalmology diagnosis.

## References

- [1] Kenneth R. Castleman: "Digital Image Processing," Prentice Hall, 1996.
- [2] Zujun Zhou: "A Review on MR Image Intensity Inhomogeneity Correction," *International Journal of Biomedical Imaging*, vol.2006, pp.1-11, 2006.
- [3] C. D. Kimmer, D. H. Ballard and J. Sklansky: "Finding Circles by An Array of Accumulators," *Communications of the ACM*, vol.18, no.2, pp.120-122, 1975.
- [4] Q. Ji and R. Q. Haralick: "Error Propagation for Hough Transform," *Pattern Recognition Letters*, vol.22, pp.813-823, 2001.
- [5] Y. Ebisawa: "Unconstrained pupil detection technique using two light sources and the image difference method," *Visualization and Intelligent Design in Engineering and Architecture II*, 15, pp.79-89, 1995.
- [6] M. D. Rafal, E. Starin and J. L. Krichmar: "Pupil detection system," *US patent 5610673*, filed in 1995.
- [7] C. Morimoto, D. Koons, A. Amir and M. Flickner: "Pupil detection and Tracking Using Multiple Light Sources," *Image and Vision Computing*, vol. 18, issue 4, pp. 331-335, 2000.
- [8] Woong-Tuk Yoo: "Pupil detection method and shape descriptor extraction method for an iris recognition, iris feature extraction apparatus and method, and iris recognition system and method using its," *US patent 2006/0147094 A1*, filed in 2004.
- [9] H. Mehrabian and P. Hashemi-Tari: "pupil boundary detection for iris recognition using graph cuts," *Proc. Image and Vision Computing*, New Zealand, pp. 77-82, Dec. 2007.
- [10] Gomai, A. El-Zaart and H. Mathkour: "A new approach for pupil detection in iris recognition system", *IEEE 2nd international conference on Computer Engineering and Technology*, pp. V4-415-419, April 2010.
- [11] M. Soltany, S. T. Zadeh and H.-R. Pourreza: "Fast and accurate positioning algorithm using circular hough transform and gray projection," *Proc. International conference on Computer Communication and Management*, 2011, Singapore, vol. 5, pp. 556-561.
- [12] A. B. Roig, M. Morales, J. Espinosa, J. Perez, D. Mas and C. Illueca: "Pupil detection and tracking for analysis of fixational eye micromovements," *Optik Int. J. Light Electron Opt.* vol. 123, pp. 11-15, 2012.
- [13] G. Akinci, E. Polat and O. M. Kocak: "A video-based eye pupil detection system for diagnosing bipolar disorder," *Proc. of 20th Signal processing and communications applications conference*, pp. 1-4, Apr. 2012.
- [14] A. Ektesabi and A. Kapoor: "Exact Pupil and Iris Boundary Detection," *Proc. 2nd International conference on control, instrumentation and automation (IC-CIA)*, pp. 1217-1221, 2011.